

Observation of anisotropy in thermoelectric properties of individual single-crystalline bismuth nanowires

Jeongmin Kim, , Jong Wook Roh, , Hongjae Moon, and , and Wooyoung Lee

Citation: *Journal of Applied Physics* **122**, 034303 (2017); doi: 10.1063/1.4994268

View online: <http://dx.doi.org/10.1063/1.4994268>

View Table of Contents: <http://aip.scitation.org/toc/jap/122/3>

Published by the *American Institute of Physics*

Articles you may be interested in

[Photo absorption enhancement in strained silicon nanowires: An atomistic study](#)

Journal of Applied Physics **122**, 034302 (2017); 10.1063/1.4993587

[Fully radiative relaxation of silicon nanocrystals in colloidal ensemble revealed by advanced treatment of decay kinetics](#)

Journal of Applied Physics **122**, 034304 (2017); 10.1063/1.4993584

[Facile design and stabilization of a novel one-dimensional silicon-based photonic crystal microcavity](#)

Journal of Applied Physics **122**, 033104 (2017); 10.1063/1.4994031

[Simplified parameter extraction method for single and back-to-back Schottky diodes fabricated on silicon-on-insulator substrates](#)

Journal of Applied Physics **122**, 034503 (2017); 10.1063/1.4994176

[Conducting wall Hall thrusters in magnetic shielding and standard configurations](#)

Journal of Applied Physics **122**, 033305 (2017); 10.1063/1.4995285

[Medical applications of hybrids made from quantum emitter and metallic nanoshell](#)

Journal of Applied Physics **122**, 034306 (2017); 10.1063/1.4994308

AIP | Journal of
Applied Physics

Save your money for your research.
It's now **FREE** to publish with us -
no page, color or publication charges apply.

Publish your research in the
Journal of Applied Physics
to claim your place in applied
physics history.

Observation of anisotropy in thermoelectric properties of individual single-crystalline bismuth nanowires

Jeongmin Kim,¹ Jong Wook Roh,² Hongjae Moon,¹ and Wooyoung Lee^{1,a)}

¹Department of Materials Science and Engineering, Yonsei University, 50 Yonsei-ro, Seodaemoon-gu, Seoul 03722, South Korea

²Inorganic Materials Lab, Samsung Advanced Institute of Technology, Samsung Electronics, 130 Samsung-ro, Suwon-si, Gyeonggi-do 16678, South Korea

(Received 10 January 2017; accepted 4 July 2017; published online 18 July 2017)

The anisotropy in the thermoelectric-transport properties of single-crystalline Bi nanowires was systematically investigated. Bi nanowires were grown along the crystal orientations of the [-102] and [100] directions using the on-film formation of nanowires method. The electrical conductivity and Seebeck coefficient of Bi nanowires with different diameters were measured with respect to temperature in both directions. The temperature dependence in electrical conductivity exhibited a significant diameter dependence, and significant anisotropy was observed in the Seebeck coefficient. Anisotropy was also observed in the thermoelectric power factor. The thermoelectric figure of merit was estimated using our previously reported thermal-conductivity data, which indicate that [100]-oriented Bi nanowires are more suitable for thermoelectric applications than [-102] nanowires. This is the first report of the anisotropy investigating all the thermoelectric-transport properties of single-crystalline Bi nanowires. *Published by AIP Publishing.*

[<http://dx.doi.org/10.1063/1.4994268>]

I. INTRODUCTION

Semimetal bismuth (Bi), which has a highly anisotropic Fermi surface originating from its rhombohedral crystal structure, has attracted considerable research interest owing to its unusual intrinsic properties such as a small band overlap (38 meV),¹ small effective mass ($\sim 0.001 m_e$),² long mean free path (~ 1 nm),³ and large Fermi wavelength (~ 70 nm).⁴ These properties lead to unique transport phenomena in nanostructured Bi, including a large magnetoresistance,^{5,6} a bipolar electrical resistivity,^{7,8} and conductive surface states.^{9,10} In particular, the single-crystalline Bi nanowire has been considered as a promising thermoelectric material owing to its unusual properties, which cause a quantum-size effect to occur easily compared with conventional metals.^{11,12} The thermoelectric property can be determined as the thermoelectric figure of merit ($ZT = S^2\sigma T/\kappa$), where T is the temperature, σ is the electrical conductivity, S is the Seebeck coefficient, and κ is the thermal conductivity.¹³ The highly anisotropic Fermi surface of Bi leads to anisotropy in the thermoelectric-transport properties, and these phenomena were intensively investigated in bulk single crystals and single-crystalline thin films.^{14–16} For nanowires, although it is expected that the anisotropic transport can be observed clearly according to the crystal orientation of the growth direction owing to the one-dimensional carrier transport, systematic investigation is considerably challenging because the crystal orientation of Bi nanowires is limited by the growth method.¹⁷ Single-crystalline Bi nanowires grown using anodic aluminum-oxide templates and the Ulitovsky method were found to be grown along the [101] and [1-11] directions,

respectively, in a hexagonal lattice.^{18,19} Therefore, the transport properties were measured along only one crystal orientation in each study.^{3,7,20,21} On the other hand, single-crystalline Bi nanowires with different crystal orientations can be grown by the on-film formation of nanowires (OFFON) method, and the anisotropy in the thermal conductivity was revealed in our previous study.²²

In the present work, we studied the electrical conductivity and Seebeck coefficient of individual single-crystalline Bi nanowires grown along the [100] and [-102] directions using the OFFON method. The anisotropy in the electrical-transport properties was systematically investigated and that in ZT was estimated using our previously reported thermal-conductivity data.²² This is the first report of the anisotropy in all the thermoelectric-transport properties and the ZT in single-crystalline Bi nanowires grown with different crystal orientations using the same method.

II. MATERIALS AND METHODS

A. Materials and characterization

Single-crystalline Bi nanowires were grown using the OFFON method, which involves the spontaneous growth of nanowires on films based on the thermal expansion mismatch between the Bi film and the substrate due to the thermally induced stress during annealing.⁶ The Bi films (< 50 nm) were deposited on a SiO₂/Si substrate by using an ultrahigh-vacuum (UHV) sputtering system (< 44 Å·s⁻¹ at 2 mTorr Ar gas). To grow the nanowires on the films, an *in situ* annealing process was conducted using an UHV furnace (5 h at 250 °C). The diameter and length of the nanowires depended on the thickness of the film and the annealing time, respectively.⁶ Figures 1(a) and 1(b) show low-magnification

^{a)}Author to whom correspondence should be addressed: wooyoung@yonsei.ac.kr

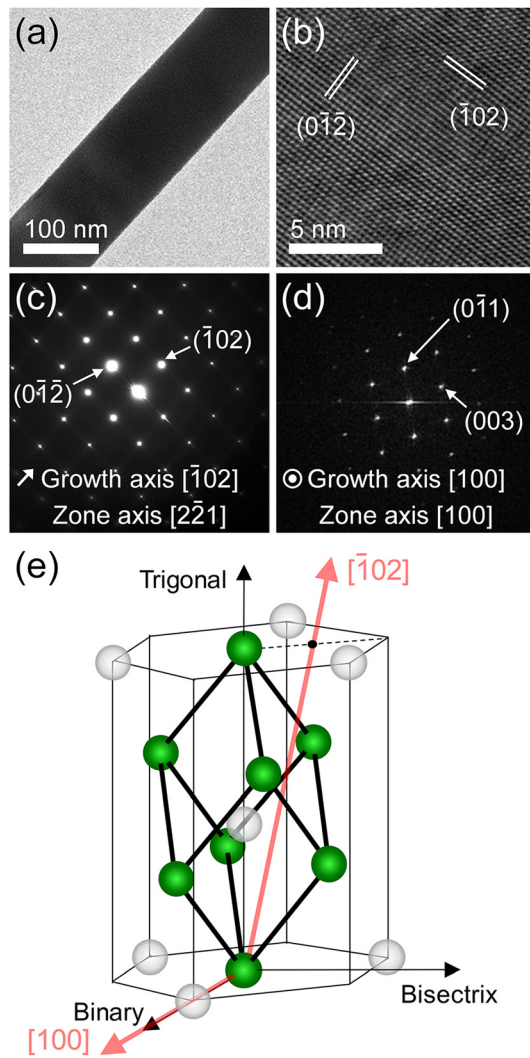


FIG. 1. Single-crystalline Bi nanowires grown by the OFFON method. (a) Low-magnification and (b) high-resolution TEM images of an as-grown Bi nanowire. (c) SAED pattern of the nanowire indicates the crystal orientation of the $[-102]$ direction. (d) SAED pattern of a Bi nanowire grown along the $[100]$ direction. The sample was prepared by slicing normal to the growth direction. (e) Schematic of the crystal structure of Bi in the hexagonal system. The two growth directions are indicated by red arrows.

and high-resolution transmission electron microscopy (TEM) images of a Bi nanowire, respectively. A selected-area electron diffraction (SAED) pattern obtained from the nanowire reveals the crystal orientation along the $[-102]$ direction, as shown in Fig. 1(c) (tilted at an angle of 10.85° with respect to the trigonal axis). Another major crystal orientation of Bi nanowires grown using the OFFON method is the $[100]$ direction (trigonal axis), which was obtained from a sample sliced normal to the growth direction by a focused ion beam [Fig. 1(d)].¹⁷ The crystal orientations of the nanowires are shown in the hexagonal lattice system of Bi in Fig. 1(e).

B. Device fabrication

Figure 2(a) shows a thermoelectric device based on an individual single-crystalline Bi nanowire. The device consists of five different electrodes, a micro-heater, a near thermometer (TM), a far TM, and resistance leads 1 and 2, which were fabricated using a typical electron-beam lithography technique

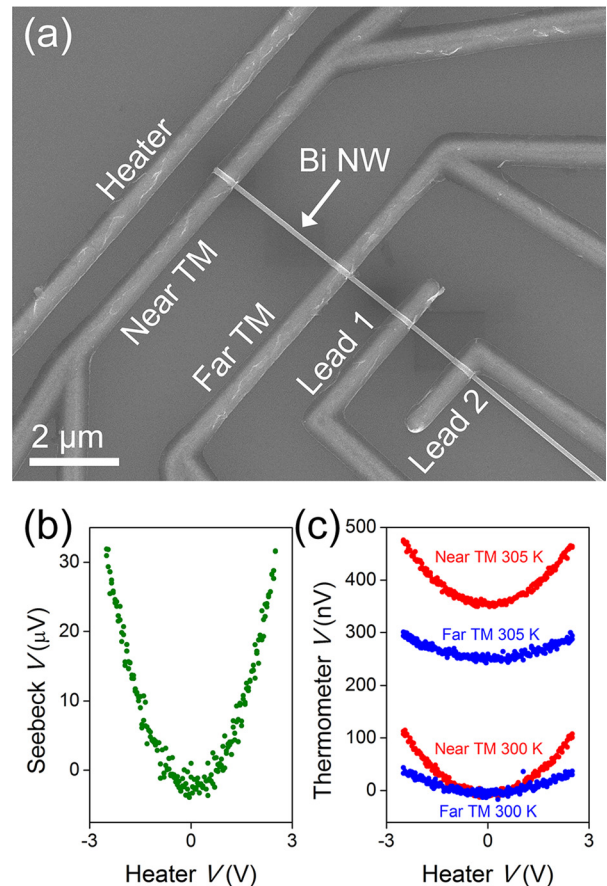


FIG. 2. Device fabrication and measurements. (a) SEM image of a thermoelectric device based on a single Bi nanowire. (b) Seebeck and (c) TM voltages obtained from the Bi nanowire with respect to the heater voltage.

and a UHV sputtering system. To obtain an Ohmic contact between the nanowire and electrodes, the oxide layer on the surface of the Bi nanowire was removed before the deposition of electrodes (Cr/Au, 5/200 nm) by Ar plasma etching using an inductively coupled plasma etching system. The device fabrication is described in detail elsewhere.^{8,10,12} In this study, thermoelectric devices with 67, 92, and 156-nm-diameter Bi nanowires grown along the $[-102]$ direction and 65, 88, and 15-nm-diameter nanowires along the $[100]$ direction were fabricated.

C. Measurement technique

The thermoelectric-transport properties (σ , S) were measured by the device using the five electrodes. The electrical conductivity was obtained using the four-probe measurement technique to determine the absolute resistance of the nanowire without a contact resistance between the nanowire and electrodes. The near TM, the far TM, lead 1, and lead 2 were used as the four terminals for the four-probe measurement. The conductivity of the nanowire was converted from the obtained resistance according to the dimensions of the nanowire. For the measurement of the Seebeck coefficient, a temperature gradient was generated by using the micro-heater. The Joule heating (P_H) induced by the heater depended on the square of the heater voltage (V_H) and the resistance of the heater (R_H), according to the relationship $P_H = V_H^2/R_H$.

Therefore, the Seebeck voltage between the near and far TMs (ΔV) was proportional to the square of the heater voltage, as shown in Fig. 2(b). The resistances of the two TMs obtained as voltage signals by using the four-probe technique were also parabolic with respect to the heater voltage because the temperature coefficient of resistance (TCR) of Au is linear in the temperature range used in this measurement [Fig. 2(c)]. To convert the TM voltages to temperatures of each TM, the measurement was performed at two different surrounding temperatures, i.e., the TCR of each TM was obtained, and the TM voltages were calibrated to the temperature difference between the two TMs (ΔT). Finally, the Seebeck coefficient of the nanowire was obtained using the relationship $S = \Delta V / \Delta T$. The measurement technique for the Seebeck coefficient in the nanowire is described in detail elsewhere.^{8,23}

III. RESULTS AND DISCUSSION

A. Anisotropic band structure of Bi

The asymmetry in the crystal structure of Bi leads to the anisotropic band structure as shown in Fig. 3(a). A large pocket of holes is along the trigonal axis at the T -point of the Brillouin zone of Bi. Three identical small pockets of electrons are tilted with respect to the bisectrix axis at about 6° at L -points.⁴ The anisotropic band structure of Bi can be determined from the effective mass components of the Fermi pockets as given in Table I.²⁴ In Table I, the three principal

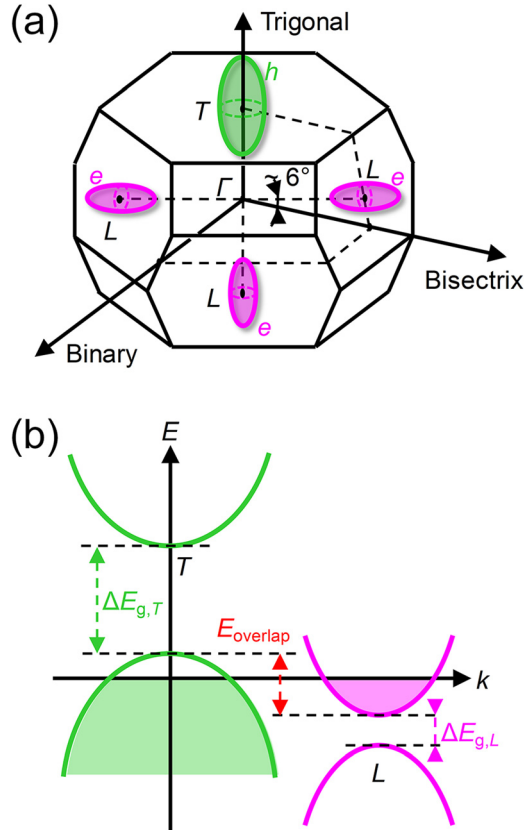


FIG. 3. Anisotropic band structure of Bi. (a) A hole pocket at the T -point and electron pockets at the L -point in the Brillouin zone. (b) Schematic of the band structure at T - and L -points.

TABLE I. Effective mass components of carrier pockets in Bi nanowires along trigonal, binary, and bisectrix axes. The unit of mass components is the free electron mass (m_0). The values of mass components were taken from Ref. 24.

Mass component		Trigonal [001]	Binary [100]	Bisectrix [-110]
L -point e -pocket (1)	m_x	0.1175	0.0023	0.0023
	m_y	0.0012	0.2659	0.0012
	m_z	0.0052	0.0012	0.2630
L -point e -pocket (2)	m_x	0.1175	0.0023	0.0023
	m_y	0.0012	0.0016	0.0048
	m_z	0.0052	0.1975	0.0666
L -point e -pocket (3)	m_x	0.1175	0.0023	0.0023
	m_y	0.0012	0.0016	0.0048
	m_z	0.0052	0.1975	0.0666
T -point h -pocket	m_x	0.0590	0.6340	0.6340
	m_y	0.0590	0.0590	0.0590
	m_z	0.6340	0.0590	0.0590

axes (trigonal, binary, and bisectrix) indicate nanowire directions, and the mass component along the nanowire direction of each pocket is denoted by m_z . Figure 3(b) shows the schematic of the Bi band structure. In bulk Bi, the valence band at the T -point and conduction band at the L -point overlap slightly, resulting in the semimetallic characteristics.¹¹ The dispersion relation for the L -point sub-bands is given by

$$E_L(k) = -\frac{\Delta E_{g,L}}{2} \pm \frac{\Delta E_{g,L}}{2} \sqrt{1 + \frac{2\hbar^2}{\Delta E_{g,L}} \left(\frac{k_x^2}{m_x} + \frac{k_y^2}{m_y} + \frac{k_z^2}{m_z} \right)}, \quad (1)$$

where $\Delta E_{g,L}$, \hbar , and k are the band gap energy of L -point sub-bands, reduced Planck's constant, and wavenumber, respectively.² The + and - signs indicate the valence and conduction bands at the L -point, respectively. In the nanowire grown along the z direction, the quantum-size effect due to the reduction in the diameter confines the carriers along the x and y directions. The band gap energy of L -point sub-bands of Bi nanowires can be expressed as

$$\Delta E_{g,L,NW}(k) = \Delta E_{g,L} \sqrt{1 + \frac{2\hbar^2}{\Delta E_{g,L}} \left(\frac{\pi^2}{m_x d^2} + \frac{\pi^2}{m_y d^2} + \frac{k_z^2}{m_z} \right)}, \quad (2)$$

where d is the nanowire diameter. Therefore, the quantum-size effect in z -oriented nanowires is determined by mass components m_x and m_y , and the change in the band structure is inversely proportional to the average of the mass components, $\tilde{m} = 2m_x m_y / (m_x + m_y)$, of each Fermi pocket. It was noted that the critical diameter at which the band overlap energy becomes zero is determined by the largest \tilde{m} of the three electron pockets. The largest \tilde{m} of three-electron pockets at L -points are calculated to be $0.0024 m_0$, $0.0046 m_0$, and $0.0031 m_0$ for the nanowires grown along trigonal, binary, and bisectrix axes, respectively, using the mass components in Table I. Therefore, the change in the band structure caused by the decrease in the diameter due to the

quantum-size effect is the largest in the trigonal Bi nanowire and smallest in the binary nanowire.²⁴

B. Electrical conductivity

Figure 4(a) shows the electrical conductivity of single-crystalline Bi nanowires grown along the [-102] and [100] directions with different diameters with respect to temperature. The room-temperature electrical conductivity was found to be 2.33×10^5 , 1.89×10^5 , and $5.81 \times 10^5 \Omega^{-1}\cdot\text{m}^{-1}$ for 156-, 92-, and 67-nm-diameter [-102] nanowires, respectively, and 1.74×10^5 , 3.08×10^5 , and $6.41 \times 10^4 \Omega^{-1}\cdot\text{m}^{-1}$

for 150-, 88-, and 65-nm-diameter [100] nanowires, respectively. In the diameter range of 50 to 200 nm, the electrical conductivity of Bi nanowires decreased with decreasing temperature.⁸ In the six nanowires used in this study, however, it is difficult to observe a clear diameter dependence for both directions because of the limited number of samples. In particular, the difference in the electrical conductivity measured from different samples increased sharply up to five-times below 100 nm, and more than 20 samples were used to determine the accurate diameter dependence of electrical conductivity in Bi nanowires.⁸ Moreover, since the anisotropy in the conductivity obtained from the bulk crystals was found to be less than about 15% ($7.4 \times 10^5 \Omega^{-1}\cdot\text{m}^{-1}$ along the [001] direction and $9.1 \times 10^5 \Omega^{-1}\cdot\text{m}^{-1}$ normal to the [001] direction),¹⁵ it was difficult to observe the anisotropy from the measured conductivity values.

On the other hand, the temperature-dependent behavior of electrical conductivity showed clear diameter dependency regardless of the growth and device fabrication methods.¹⁷ Therefore, the values of electrical conductivity were normalized by the room-temperature conductivity for comparison [Fig. 4(a)]. In both directions, the temperature dependence of the electrical conductivity varied from metallic to semiconducting as the diameter decreased, which agrees well with the results of a previous study.⁸ Generally, the electrical conductivity in metals increases as the temperature decreases, which is attributed to the temperature dependence of carrier mobility. However, in semiconductors, the decrease in the carrier density results in the decrease in the electrical conductivity with decreasing temperature. In semimetal Bi, the two aforementioned characteristics coexist because of the small carrier density ($3.0 \times 10^{18} \text{cm}^{-3}$),¹ and the electrical conductivity is determined by the competition between temperature dependences of the carrier mobility and density.⁸ As the diameter decreases, the mobility contribution to the temperature-dependent conductivity decreases owing to the carrier surface scattering caused by the classical size effect.¹⁰ Furthermore, the decrease in the band overlap energy caused by the quantum-size effect increases the effective mass of electrons and decreases the carrier density, resulting in the semiconducting characteristics with the decreasing diameter.¹² As described above, the decrease in the band overlap energy due to the quantum-size effect depended on the crystal orientation of the nanowire and was calculated to be most significant along the [001] direction and least along the normal to the [001] direction.²⁴ Therefore, the electrical conductivity of the 67-nm-diameter [-102] nanowire decreases more sharply compared to that of the 65-nm-diameter [100] nanowire.

C. Seebeck coefficient

Figure 4(b) shows the temperature dependence of the Seebeck coefficient of the Bi nanowires grown along the [-102] and [100] directions with different diameters. In both directions, the Seebeck coefficients, which represent the entropy carried per unit charge, converge to zero at the absolute temperature.²³ In two-band systems such as semimetal Bi, the Seebeck coefficient is defined as follows: $S_{\text{total}} = (\sigma_1 S_1 + \sigma_2 S_2) / (\sigma_1 + \sigma_2)$, where the subscripts 1 and 2 indicate two sub-bands.²⁵ The

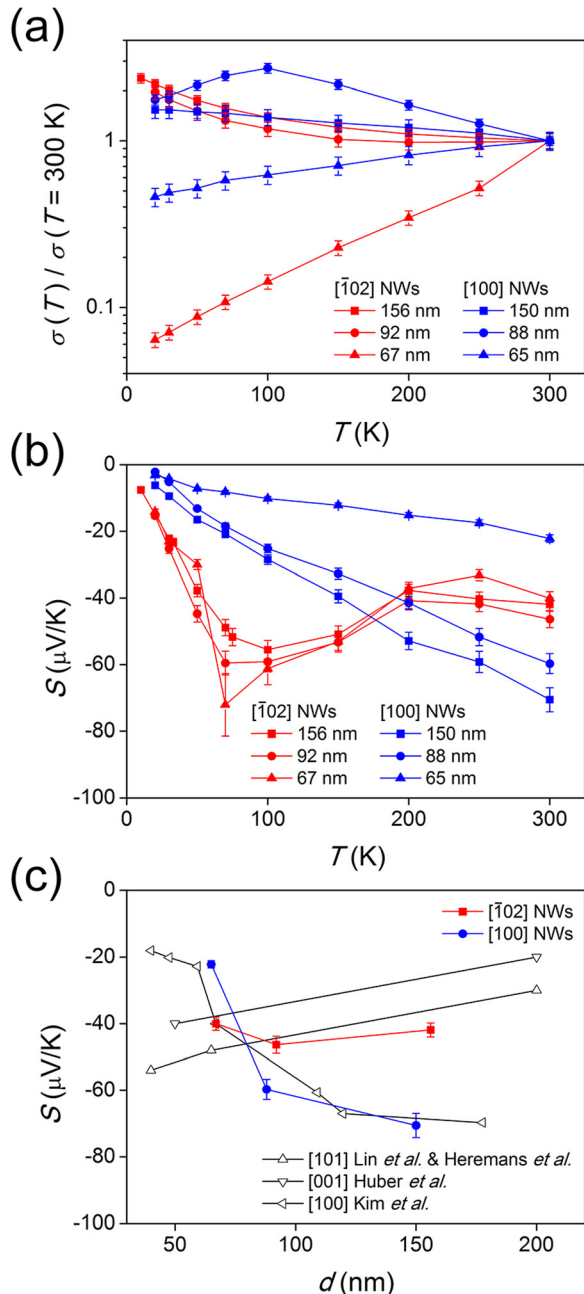


FIG. 4. Electrical-transport properties of Bi nanowires grown along the [-102] and [100] directions. (a) Normalized electrical conductivity and (b) Seebeck coefficient were obtained with respect to the temperature for different diameters. (c) Diameter dependence of the Seebeck coefficient at 300 K. The values measured by Heremans *et al.*, Kim *et al.*, Lin *et al.*, and Huber *et al.* were taken from Refs. 7, 8, 27, and 28, respectively.

weighting factors, i.e., the partial electrical conductivities of each band, determine the contribution of the partial Seebeck coefficient to the total Seebeck coefficient. In Bi, the total Seebeck coefficient is considerably sensitive to the weighting factors because the partial Seebeck coefficients of the valence band at the T -point (hole) and conduction band at the L -point (electron) are positive and negative, respectively.^{7,26} Therefore, the change in the electrical-transport properties caused by the diameter decrease due to the quantum-size effect lead to the variation in the Seebeck coefficient. However, in the $[-102]$ -oriented nanowires, the absolute values of the Seebeck coefficient increased without the diameter dependence as the temperature neared 100 K, while the $[100]$ -oriented nanowires showed a linear temperature dependence and a clear diameter dependence, as reported in a previous study.⁸ This can be attributed to the anisotropic band structure of Bi. The carrier mobility, which determines the weighting factor of the partial Seebeck coefficient, is proportional to the carrier mean free path ℓ and reversely proportional to the carrier effective mass m^* ($\mu \propto \ell/m^*$). Therefore, when the difference between effective masses of the hole and electron is large, the difference between the hole and electron carrier mobilities becomes sensitive to ℓ . In contrast, the difference between the mobilities is sensitive to m^* when the difference in effective masses is small. The effective masses of holes along the nanowire direction ($m_{z,T}$) is $0.634 m_0$ and $0.059 m_0$ for the trigonal and binary directions, respectively (Table I). The average effective masses of three pockets was calculated to be $0.0017 m_0$ and $0.0012 m_0$ for the trigonal and binary directions, respectively, by using Matthiessen's rule ($\tilde{m}_{z,L} = 1/((1/m_{z,L1}) + (1/m_{z,L2}) + (1/m_{z,L3}))$). The difference between the hole and electron carrier effective masses is about 10 times larger in the trigonal direction than that in the binary direction. Therefore, the total Seebeck coefficient is sensitive to ℓ as it approaches the trigonal direction, and it is more sensitive to the effective mass as it approaches the binary direction. Thus, $[100]$ -oriented nanowires show a clear diameter dependence due to the increase in the effective mass caused by the change in the band structure,¹² compared to the nanowires with the z -index as shown in Fig. 4(c).^{7,8,27,28} In the case of the $[-102]$ -oriented nanowire, the Seebeck coefficient increases with decreasing temperature because the effect of temperature-dependent ℓ on mobility is larger in electrons than in holes.

D. Power factor

The power factor of the $[-102]$ and $[100]$ -oriented Bi nanowires, which indicates the electrical thermoelectric performance of materials and is proportional to the electrical conductivity and the square of the Seebeck coefficient ($S^2\sigma$), is presented in Fig. 5(a). For the $[-102]$ nanowires, the power factor was optimized in the low-temperature region, where the increase in the Seebeck coefficient was observed. However, for the $[100]$ nanowires, the power factor was maximized at 300 K owing to the linear temperature dependence of the Seebeck coefficient. Moreover, a clear diameter dependence was observed, as indicated by the Seebeck coefficient. However, the diameter dependence of the electrical

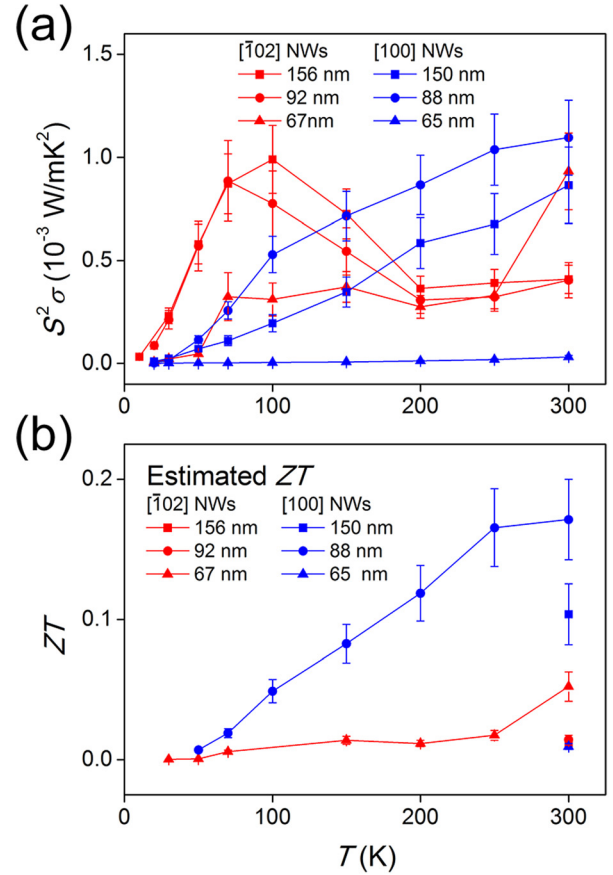


FIG. 5. Thermoelectric-transport properties of Bi nanowires grown along the $[-102]$ and $[100]$ directions. (a) Thermoelectric power factor was obtained with respect to the temperature for different diameters. (b) Temperature-dependent ZT was estimated using our previously reported thermal-conductivity data, which are given in Ref. 22.

conductivity dominated that of the power factor. In particular, the 65-nm nanowire showed a significantly small power factor compared with the others owing to the semiconducting transport characteristics.

E. ZT estimation

Finally, the anisotropy of the thermoelectric figure of merit was investigated. To estimate the ZT according to the obtained power factor, the thermal-conductivity data for single-crystalline Bi nanowires grown by an identical method were taken from our previous study on the anisotropy in the thermal conductivity.²² In the previous study, although the diameter-dependent thermal conductivity was fully investigated at 300 K in the diameter range wherein the power factor was obtained, few nanowires were measured over the full temperature range (30–300 K). Therefore, the ZT values of the 67-nm-diameter $[-102]$ - and 88-nm-diameter $[100]$ -oriented nanowires were estimated in the full temperature range, but those of the other nanowires were obtained at 300 K, as shown in Fig. 5(b). Except for the 65-nm nanowire, which showed a significantly low electrical conductivity, in the measured temperature range, the ZT was higher in the $[100]$ -oriented nanowires than in the $[-102]$ nanowires. This is attributed to not only the anisotropy in the power factor but also the thermal conductivity: the thermal conductivity of the $[-102]$ -oriented

nanowires was 4-fold higher than that of the [100] nanowires at the same diameter.²² Although the anisotropic thermal conductivity was also observed in bulk crystals along the directions parallel and perpendicular to the trigonal direction, the temperature-dependent thermal conductivity in nanowires showed a trend opposite to that observed in the bulk.^{15,22} This indicates that phonon surface scattering is significant in thermal conductivity as well as carrier surface scattering in nanowires.²² Therefore, the deviation in the thermal conductivity between the [-102]- and [100]-oriented nanowires may be due to different phonon surface scattering parameters along the two directions originating from the highly anisotropic crystal structure.²² The enhancement of the power factor in the low-temperature region can increase the ZT of 92- and 156-nm-diameter [-102]-oriented nanowires. However, it is expected that the optimized ZT cannot exceed that of the [100] nanowires, owing to the high thermal conductivity of the [-102] nanowires.

IV. CONCLUSION

We observed the anisotropy in the thermoelectric-transport properties of single-crystalline Bi nanowires grown along the crystal orientations of the [-102] and [100] directions using the OFFON method. The electrical conductivity and Seebeck coefficient of the Bi nanowires were measured with respect to the temperature on Si/SiO₂ substrates using a typical electron-beam lithography technique. Diameter-dependent properties were observed in two different growth directions. To evaluate the thermoelectric performance, the ZT of the nanowires was estimated using our previously reported thermal conductivity data obtained from nanowires grown by using an identical method. The temperature dependence in electrical conductivity exhibited a significant diameter dependence in both directions, and significant anisotropy was observed in the Seebeck coefficient. Moreover, the thermoelectric power factor showed anisotropy, and the estimated ZT indicated that the [100]-oriented Bi nanowires are more suitable for thermoelectric applications than the [-102] nanowires. This is the first report of the anisotropy in all the thermoelectric-transport properties in single-crystalline Bi nanowires with different crystal orientations grown by the same method.

ACKNOWLEDGMENTS

This work was supported by the National Research Foundation of Korea (NRF) grant funded by the Korea

government (MSIP) (2014R1A2A1A10053869) and the Priority Research Centers Program (2009-0093823).

- ¹Z. B. Zhang, X. Z. Sun, M. S. Dresselhaus, J. Y. Ying, and J. Heremans, *Phys. Rev. B* **61**, 4850 (2000).
- ²S. B. Cronin, Ph.D. thesis (Massachusetts Institute of Technology, 2002).
- ³J. Heremans, C. M. Thrush, Y. M. Lin, S. Cronin, Z. Zhang, M. S. Dresselhaus, and J. F. Mansfield, *Phys. Rev. B* **61**, 2921 (2000).
- ⁴T. W. Cornelius and M. E. T. Molares, *Nanowires* (InTech, Shanghai, 2010), Vol. 14.
- ⁵F. Y. Yang, K. Liu, K. M. Hong, D. H. Reich, P. C. Searson, and C. L. Chien, *Science* **284**, 1335 (1999).
- ⁶W. Shim, J. Ham, K. I. Lee, W. Y. Jeung, M. Johnson, and W. Lee, *Nano Lett.* **9**, 18 (2009).
- ⁷J. Heremans and C. M. Thrush, *Phys. Rev. B* **59**, 12579 (1999).
- ⁸J. Kim, S. Lee, Y. M. Brovman, P. Kim, and W. Lee, *Nanoscale* **7**, 5053 (2015).
- ⁹P. Hofmann, *Prog. Surf. Sci.* **81**, 191 (2006).
- ¹⁰J. Kim, S. Lee, Y. M. Brovman, M. Kim, P. Kim, and W. Lee, *Appl. Phys. Lett.* **104**, 043105 (2014).
- ¹¹M. S. Dresselhaus, G. Dresselhaus, X. Sun, Z. Zhang, S. B. Cronin, and T. Koga, *Phys. Solid State* **41**, 679 (1999).
- ¹²J. Kim, D. Kim, T. Chang, and W. Lee, *Appl. Phys. Lett.* **105**, 123107 (2014).
- ¹³H. J. Goldsmid, *Thermoelectric Refrigeration* (Plenum Press, New York, 1964).
- ¹⁴B. S. Chandrasekhar, *J. Phys. Chem. Solids* **11**, 268 (1959).
- ¹⁵C. F. Gallo, B. S. Chandrasekhar, and P. H. Sutter, *J. Appl. Phys.* **34**, 144 (1963).
- ¹⁶F. Y. Yang, K. Liu, K. Hong, D. H. Reich, P. C. Searson, C. L. Chien, Y. Leprince-Wang, K. Yu-Zhang, and K. Han, *Phys. Rev. B -Condens. Matter Mater. Phys.* **61**, 6631 (2000).
- ¹⁷J. Kim, W. Shim, and W. Lee, *J. Mater. Chem. C* **3**, 11999 (2015).
- ¹⁸Z. Zhang, X. Sun, M. S. Dresselhaus, J. Y. Ying, and J. P. Heremans, *Appl. Phys. Lett.* **73**, 1589 (1998).
- ¹⁹A. Nikolaeva, D. Gitsu, L. Konopko, M. J. Graf, and T. E. Huber, *Phys. Rev. B* **77**, 075332 (2008).
- ²⁰L. Konopko, T. Huber, and A. Nikolaeva, *J. Low Temp. Phys.* **159**, 253 (2010).
- ²¹D. Gitsu, L. Konopko, A. Nikolaeva, and T. E. Huber, *Appl. Phys. Lett.* **86**, 102105 (2005).
- ²²J. W. Roh, K. Hippalgaonkar, J. H. Ham, R. K. Chen, M. Z. Li, P. Ercius, A. Majumdar, W. Kim, and W. Lee, *ACS Nano* **5**, 3954 (2011).
- ²³Y. M. Zuev, W. Chang, and P. Kim, *Phys. Rev. Lett.* **102**, 096807 (2009).
- ²⁴Y. M. Lin, X. Z. Sun, and M. S. Dresselhaus, *Phys. Rev. B* **62**, 4610 (2000).
- ²⁵L. D. Hicks and M. S. Dresselhaus, *Phys. Rev. B* **47**, 12727 (1993).
- ²⁶J. P. Heremans, C. M. Thrush, D. T. Morelli, and M.-C. Wu, *Phys. Rev. Lett.* **88**, 216801 (2002).
- ²⁷Y.-M. Lin, O. Rabin, S. B. Cronin, J. Y. Ying, and M. S. Dresselhaus, *Appl. Phys. Lett.* **81**, 2403 (2002).
- ²⁸T. E. Huber, A. Adeyeye, A. Nikolaeva, L. Konopko, R. C. Johnson, and M. J. Graf, *Phys. Rev. B* **83**, 235414 (2011).